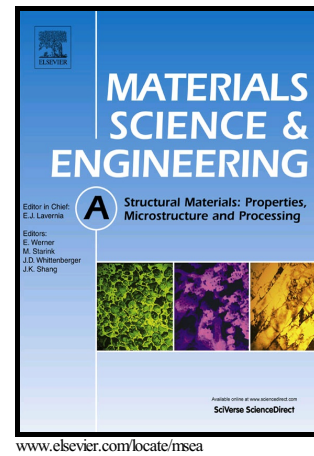# Author's Accepted Manuscript

Effect of ECAP processing on microstructure evolution and dynamic compressive behavior at different temperatures in an Al-Zn-Mg alloy

Mohamed A. Afifi, Pedro Henrique R. Pereira, Ying Chun Wang, Yangwei Wang, Shukui Li, Terence G. Langdon

Effect of ECAP processing on microstructure evolution and dynamic compressive

behavior at different temperatures in an Al-Zn-Mg alloy

Mohamed A. Afifi[a], Pedro Henrique R. Pereira[b], Ying Chun Wang[a,c*],Yangwei Wang[a], Shukui Li[a,c], Terence G. Langdon[b]

[a]School of Materials Science and Engineering, Beijing Institute of Technology, Beijing 100081,China
[b]Materials Research Group, Faculty of Engineering and the Environment, University of Southampton, Southampton SO17 1BJ, U.K.
[c]National Key Laboratory of Science and Technology on Materials under Shock and Impact, Beijing 100081,China

[*]Corresponding author: Ying Chun Wang, Tel: 861068913937 ext.801. e-mail: wangyc@bit.edu.cn

Abstract

An artificially aged Al-Zn-Mg alloy with a grain size of ~ 1.3 μm was processed by equal-channel angular pressing (ECAP) and then subjected to dynamic compression at a strain rate of 4000 s^{-1} in the range from room temperature to 673 K. The results show the η′ phase is refined and a η phase is formed during the first pass of ECAP and after further processing 8 passes the GP zones are removed. An ultrafine-grained (UFG) structure with an average grain size of ~200 nm was obtained after 4 passes. It is shown that dynamic compressive deformation assists the precipitation process through precipitate coalescence and by changing the precipitate orientations. The dynamic compressive yield strengths and flow stresses decrease gradually to different degrees with increasing temperature except after ECAP processing for 4 passes where there is thermal stability up to 473 K. The ECAP processing significantly improves the strength of the alloy at elevated temperatures by comparison with the as-received material.

1. Introduction

Al-Zn-Mg alloys are used extensively as structural materials in the aerospace and automobile industries due to their high strength-to-weight ratio. There is nevertheless much interest in further enhancing the mechanical properties of these alloys [1-4]. It is well-known that the ultrafine-grained (UFG) materials produced by severe plastic deformation (SPD) processing exhibit significantly higher strength by comparison with their coarse grained (CG) counterparts [5-7]. Among the various SPD processing methods, equal-channel angular pressing (ECAP) is especially attractive because it can be scaled-up relatively easily to produce large bulk UFG materials that may be used in structural applications [8].

Early research on the ECAP processing of Al alloys was generally focused on the significance of the grain refinement [9-12]. More recently, there is a growing interest in investigating the coupling effect of grain refinement and the introduction of dislocations and precipitation on the strength of Al alloys [13,14]. Very recent experiments showed that a UFG 7075 alloy processed by ECAP for only 4 passes achieved maximum tensile properties due to the presence of many fine η′ phases and minor quantities of GP zones distributed in fine grains having a size of less than 600 nm [15]. Another study showed that the yield strength of the 7005 alloy was remarkably increased after 7 ECAP passes due to a combination of precipitation strengthening, dislocation strengthening and grain boundary strengthening [16].

To date, many researchers have studied the quasi-static mechanical properties of these UFG precipitate-hardened Al alloys processed by ECAP including Al-Zn-Mg alloys Nevertheless, only very limited information is at present available on the dynamic properties of UFG Al-Zn-

1

Mg alloys [17] although this information is an important prerequisite for making use of these alloys in many structural applications. For example, during subsequent service these alloys are often subjected to dynamic shock loading as in an automobile crash or when a bird strikes an aircraft fuselage or wing during operation. Therefore, it is important to determine the dynamic response of these alloys in impact loading.

Accordingly, the aim of this research was to investigate the effect of ECAP processing on the dynamic mechanical properties of an Al-Zn-Mg alloy over the temperature range from room temperature (RT) to 673 K. In addition, the microstructural evolution, including grain size and the presence of dislocations and precipitates, was studied before and after dynamic compression.

2. Experimental material and procedures

The experiments used an Al-Zn-Mg alloy having a chemical composition, in wt. %, of Al-4.6Zn-2.58Mg-0.35Mn-0.2Cr. The alloy was received as a plate with a thickness of 22 mm following solution treatment at 743 K for 1 h and then artificial aging at 393 K for 24 h (T6 treatment): this is designated the as-received condition. Billets with 9.8 mm diameter and 65 mm length were machined from the plates and then processed by 1, 4 or 8 passes of ECAP using route B_c in which the sample is rotated by 90° in the same sense between each pass [18]. The ECAP was conducted at 423 K using a pressing speed of 2 mm s^{-1} and a solid die with an internal channel angle of 90° and an outer arc of curvature of 20° so that a strain of ~1 was imposed on the sample in each separate pass [19].

For dynamic testing, cylindrical specimens with diameters of 5 mm and heights of 4 mm were cut from both the ECAP-processed billets along the pressing direction and the as-received Al-Zn-Mg alloy plate. Dynamic compression testing was carried out at various temperatures from RT to 673 K at a strain rate of 4000 s^{-1} using a conventional split Hopkinson pressure bar

2

(SHPB) described earlier [20]. Elevated temperatures were obtained using a small furnace placed between the input and output bars of the SHPB setup. Before the dynamic testing, each specimen was held at the required temperature for 10 min to ensure a uniform temperature distribution throughout the sample. The microstructures of the as-received and the ECAP-processed alloy were characterized before and after dynamic compression using transmission electron microscopy (TEM) with an F20 Field Emission TEM and JEM 2100 LaB_6 operating at 200 kV. For TEM characterization, thin foils of the materials were cut from the cross-sections of each billet which are perpendicular to the pressing direction. The foils were thinned to ~110 μm by mechanical grinding using grit papers ranging from 800 to 2000 mesh followed by thinning to electron transparency using a Gatan Dual Ion Milling System. The dislocation densities were evaluated using a D8 Advanced Bruker X-ray diffraction (XRD) facility.

3. Experimental results

3.1 Dynamic mechanical properties

The true stress-true strain curves of the as-received and the ECAP-processed alloy are shown in Fig. 1 for temperatures from RT to 673 K at a strain rate of 4000 s^{-1}: the plots in Fig. 1 are for (a) the as-received condition and after ECAP processing through (b) 1, (c) 4 and (d) 8 passes. It is readily apparent that the dynamic compressive yield strengths and flow stresses decrease gradually with increasing temperature. The reduction in the yield stress for the as-received alloy between RT and 673 K is ~300 MPa whereas after ECAP processing for 1, 4 and 8 passes the decrements are ~250, ~150 and ~180 MPa, respectively. The temperature sensitivity of the yield strength and the flow stress are reduced after ECAP processing. Moreover, the flow stresses of the alloy subjected to ECAP processing for 4 passes in Fig. 1(c) exhibit thermal stability up to 473 K.

By comparison, the alloy processed by ECAP has higher strength than the as-received material. The yield strength and peak stress of samples processed through 1 pass of ECAP at RT are 590 and 640 MPa, respectively, and this is higher than for the as-received material. At the higher temperatures, the alloy possesses a much higher strength after ECAP processing than in the as-received condition. Thus, the yield strength and peak stress after ECAP for 4 passes at 373 K are approximately 25% and 12% higher than the as-received material but these numbers are increased to 50% and 40% at 673 K. In addition, there is only a minor difference in the flow stresses at RT for the samples processed by different numbers of ECAP passes although the alloy subjected to 4 ECAP passes exhibits the highest strength at elevated temperatures.

3.2 Microstructure characterization before dynamic testing

Typical microstructures of the alloy before dynamic testing are depicted in Fig. 2 for (a) the as-received condition and after ECAP through (b) 1, (c) 4 and (d) 8 passes. It is apparent from Fig. 2(a) that the as-received material has an average grain size of ~1.3 μm with a large number of precipitates of ~120 nm in length distributed reasonably homogeneously and a few dislocations observed near some grain boundaries. The precipitates for these same samples are shown by the higher magnification images including the selected area electron diffraction (SAED) patterns in Fig.3. In Fig. 3(a) the precipitates in the as-received alloy are mainly GP zones and coarse η′ phases as verified by the SAED pattern. Diffraction spots were observed in the <322> zone axis where diffuse spots of GP zones at 1/3 {133} were present with η′ spots [21,22]. The microstructure after 1 pass of ECAP in Fig. 2(b) shows an elongated dislocation cell structure having a few platelet precipitates with the same size as observed in the as-received material in Fig.2(a) . Numerous very fine spherical precipitates, verified by Fig.3 (b) in which

indexing along <110> shows the presence of some GP zones as well as η′ and a few η phases [21-23].

Figure 2(c) reveals the presence of well-defined equiaxed grains after ECAP for 4 passes and this replaces the band-like dislocations substructure. Also, these precipitates are predominantly η′ and η phases with weak spots of few retained GP zones as verified along <112> in the diffraction pattern displayed in Fig. 3 (c). The weak diffraction at {311}/2 is from GP (II) zones [24] and the diffraction spots close to {111} are from η′ and η at ¾{220} [25,26]. Finally, it is apparent from Fig. 2 (d) that further ECAP processing to 8 passes leads to additional grain refinement and, in addition, it is apparent from Fig. 3 (d) that the sizes of the dominant precipitates are slightly increased. The precipitation spots are in the orientations of $η′_2$ and $η_1$ [27,28].

The average grain sizes of the samples subjected to 4 and 8 passes of ECAP were estimated using the linear intercept method and the mean grain sizes were ~200 and ~190 nm after 4 and 8 passes, respectively. The dislocation densities were estimated by XRD using the modified Williamson-Hall method [29] and the values were 2.5×10^{13}, 3.5×10^{14}, 3.2×10^{14} and $3.3 \times 10^{14} \, m^{-2}$ for the as-received and after processing through 1, 4 and 8 passes, respectively. For convenience, the microstructural features in Figs. 2 and 3 are summarized in Table 1.

3.3 Microstructures after dynamic testing

Figure 4 shows typical TEM micrographs of the as-received and the ECAP-processed alloy after dynamic testing at a strain rate of ~4000 s^{-1} at RT (top row), 473 (middle row) and 673 K (bottom row), respectively. Fig.5 (a)-(l) shows the corresponding SAED of Fig.4 (a)-(l). Fig. 4(a) shows that the microstructure of the as-received alloy tested at RT exhibits a high density of dislocations and precipitates mainly in the form of η′ phases and GP zones, and this is confirmed

5

by the SAED shown in Fig. 5(a) along <411> containing diffraction of η'_2 along <011> and GP zones at {1,1/4,0} [24,27]. The dislocation density is reduced and the precipitates are in the form of η' and η after testing at 473 K in Fig. 4(e) and finally the formation of equiaxed grains due to partial dynamic recrystallization is evident at 673 K in Fig. 4(i). Patterns associated with η' and η are shown in Fig. 5(e) along <112> and Fig. 5(i) along <011> projections [22,24,30]. An example of a coarse precipitate of ~35 nm is shown in Fig. 6(a) which has a hexagonal η' as examined through fast Fourier transform (FFT).

For the alloy subjected to 1 pass of ECAP, the microstructure after dynamic testing at RT shown in Fig. 4(b) exhibits tangled dislocations with fine η' precipitates, as proven by the corresponding <110> SAED in Fig. 5(b). New subgrains and a lower dislocation density are observed at 473 K in Fig. 4(f) where the precipitates in the matrix are primarily in the form of η' precipitates with some precipitation of η as indexed in Fig. 5(f). At 673 K there is a polygonized structure with a high density of dislocations as shown in Fig. 4(j). The corresponding SAED shows diffraction spots of precipitates scattered along the white ring patterns of the η' and η [25]. Experimental evidence of precipitate coalescence at 673 K is shown in Fig. 6(b) for the merging of two η' precipitates.

Figures 4(c) and (g) show the microstructures of the alloy after 4 passes of ECAP followed by dynamic testing at RT and 473 K, respectively. These images reveal the presence of high dislocation densities arranged in the form of tangles. The precipitations are mainly η' and η as observed in Fig. 5(c) and 5(g). At 673 K equiaxed grains are visible with an average size of ~900 nm as shown in Fig. 4(k). In addition, the η' and η phases are coarsened at 673 K which display random orientations along <110> as shown in Fig. 5(k). The diffracted spots located in the first circle to the center spot belong to η' along {1121} and {0008}. The outer circles spots are

referred to η which displays different orientations with the presence of GP zones along {311}/2 [22,25].

The microstructures of the alloy processed by 8 passes of ECAP and tested dynamically are shown in Fig. 4(d), (h) and (l). In Fig. 4(h) there are a small number of small equiaxed grains formed due to recrystallization when testing at 473 K. Equiaxed grains are also formed with an average grain size of ~800 nm at 673 K in Fig. 4(l). Spots of η′ and η are observed along <112> and <110> in Fig.5(d) and Fig.5(h), respectively. In addition, there are high densities of precipitates consisting of η′ and η phases after dynamic deformation at temperatures from RT to 673 K. Inspection of the SAED pattern in Fig. 5(l) shows a circle of GP zones, η′ and η precipitates. The first circle surrounding the central spot refers to η′ precipitates along $\{11\overline{2}0\}$, the second circle is for the η′ and GP zones and the outward 3 rings refer to η precipitates [22,25-26]. The presence of GP zones in the diffraction patterns of Figs. 5(k) and 5(l) suggest dynamic precipitation (DPN) as there are no GP zones before testing in Fig. 3. Furthermore, the presence of η phases along different diffraction rings indicates that these precipitates have different orientations which indicate that the accumulated strain produced by dynamic compression significantly alters the η orientations.

4. Discussion

4.1 Precipitation evolution during ECAP

The precipitation evolution during ECAP processing is significantly different from the as-received Al-Zn-Mg alloy. The corresponding SAED patterns in Fig. 3 reveal that the dominant precipitates are η′ and η after ECAP for 4 and 8 passes while GP zones and η′ phases are predominant for the material subjected to a single ECAP pass and also for the as-received material. Moreover, the size of a majority of the η′ precipitates is significantly decreased after 1

7

ECAP pass which may be a direct consequence of shearing of the η′ precipitates by dislocations during the ECAP processing as observed in Fig. 3 (b) or the formation of new η′ precipitates from GP zones [26,31]. Precipitation fragmentation during ECAP was also reported earlier in Al-Cu, Al-Mg-Si and 7034 alloys [32-34]. Thus, increasing the ECAP to 4 passes means that the η phases are formed and there is a further increase in size with increasing to 8 passes.

The absence of GP zones after ECAP for 8 passes confirms that the precipitation process transforms the GP zones to η′ and η with subsequent coarsening. The size of η′ grows by ~60% when increasing the ECAP passes from 1 to 8. Therefore, it is concluded that ECAP processing affects the precipitation thermodynamics by promoting isotropic growth and by forming equiaxed η precipitates [26].

4.2 Precipitation evolution during dynamic compression

With increasing temperature for dynamic testing, the η′ precipitates grow slightly and η particles appear for both the as-received alloy and after ECAP processing for 1 pass. The coalescence of two η′ precipitates was observed in the ECAP processed material after 1 pass at 673 K as shown in Fig. 6(b). This demonstrates that precipitates may merge and coarsen during dynamic testing.

GP zones were observed in the alloy after 8 passes of ECAP and further dynamic testing. However, these solute-enriched regions were not found before dynamic testing in the alloy processed by ECAP for 8 passes. In addition, dislocations can assist DPN through the formation of lath-like η by pipe diffusion paths that increase the overall diffusion rate [35]. Accordingly, Fig. 4(l) shows lath-like η in or close to dislocations.

The microstructure of the alloy subjected to ECAP processing and further dynamic testing at 673 K contained coarser precipitates than the other tested samples and this ultimately leads to

a more random orientation of the η phase as shown in Fig. 5. This may be attributed to an increase in the surface energy at the interface between the precipitates and the matrix after SPD whereby the higher energy at the interface promotes the growth of precipitates [26]. The coarsening of precipitates may also be attributed to the higher dislocation density during ECAP for additional 4 passes. It has been proposed that the nucleation and coarsening of precipitates may be assisted by dislocations through a heterogeneous nucleation process [36].

4.3 Temperature dependence of the dynamic compressive properties

The temperature dependence of the yield strength in the Al-Zn-Mg alloy subjected to dynamic testing in the as-received and the ECAP-processed condition is depicted in Fig. 7. Thus, increasing the testing temperature from RT to 673 K leads to a gradual decrease of the yield strength in the as-received alloy and in the material processed by 1 ECAP pass. Part of the strength in the as-received alloy comes from a restriction to dislocation motion due to the large number of GP zones in addition to the lattice strain interactions between precipitates of semi-coherent η′ and the dislocations. Therefore, increasing the testing temperature accelerates the rate of dislocation annihilation and ultimately leads to a reduction in yield strength. After ECAP for 1 pass, the increase in strength over the as-received alloy is attributed to the higher density of dislocations and the finer GP zones and η′. Furthermore, the yield strength after 1 pass of ECAP also decreases as a result of recovery similar to the as-received material.

By contrast, the UFG structure with a large number of precipitates obtained by ECAP for 4 passes possesses an exceptional thermal stability at temperatures up to 473 K. The reason for this stability may be evaluated by considering the precipitation during dynamic testing at different temperatures. There are no overall differences in the microstructure of the alloy subjected to 4 passes of ECAP and further dynamic testing within the temperature interval from RT to 473 K.

9

After dynamic straining over this temperature range, it is readily apparent from the TEM images displayed in Figs. 4(c) and (g) that the presence of fine precipitates effectively pins the grain boundaries and dislocations and therefore the migration rate of grain boundaries and dislocations is restricted. The situation is different after 8 passes of ECAP as the coarser precipitates observed in Figs. 4(h) and (l) provide a lower drag force to hinder the grain boundary and dislocation movement and the material partially recrystallizes at 473 K as in Fig. 4(h).

The mechanical strength of the alloy after 4 and 8 passes of ECAP and further dynamic testing at 673 K is improved by comparison with both the as-received alloy and the alloy processed by ECAP for 1 pass because the spheroidal precipitates effectively prevent grain growth and η provides the presence of athermal long range barriers for dislocation movement. The flow stresses are up to ~150 MPa higher than in the as-received material after ECAP through 4 passes and dynamic straining at temperature from 373 to 673 K. Accordingly, it is concluded that SPD processing is a valuable procedure for producing automotive components such as sensors and actuators that will be used in high temperature environments.

4.4 The work hardening rates

In order to compare the work hardening and dynamic softening at different testing temperatures, the work hardening rate, θ (= $d\sigma/d\varepsilon$, where σ is the true stress and ε is the true strain), is plotted as a function of the true strain for various conditions in Fig. 8. It is evident that the relation of θ to strain can be divided into three stages at all experimental conditions following strain hardening theory [37-39]. Initially, the value of θ is positive at low strains when dislocation accumulation is dominant. With further straining θ decreases until it reaches zero value indicating a balance between strain hardening and dynamic softening at this point. This is followed by stage II which is characterized by fluctuations of θ around the zero line. Generally in

this stage the strain hardening is slightly greater than dynamic softening and it is also shown in Fig.1 that the flow stress further slightly increases with strain increasing in the same strain range. The apparent wave-like perturbations of the work hardening rates are probably due to variations in the rates of dynamic recovery and dislocation accumulation in the presence of non-shearable precipitates which also acts as a hardening mechanism [40-43]. Stage III is initiated when the values of θ become zero at a certain strain and is maintained negative with further straining. In this final stage, dynamic softening is caused by dynamic recovery or dynamic recrystallization may be overwhelming [44].

The starting point of stage III represents the beginning of dynamic softening and this is sensitive to the testing temperature and ECAP processing. An examination of the values of the starting strain for stage III for the as-received and the ECAP-processed materials in Fig.8 shows that the sample at 4 passes possesses the highest resistance to dynamic softening when tested at RT and 473 K because the strains are 0.32 and 0.34, respectively, and these values are higher than any other experimental conditions. This is consistent with the exceptional thermal stability of the alloy processed by ECAP for 4P at temperatures up to 473 K as shown in Fig.7 and analyzed by evaluating Fig.4(c) and (g). However, the starting strain of dynamic softening tested at 673 K for the alloy after ECAP for 1, 4 and 8 passes decreases to no more than ~0.22 and this is lower than the as-received material with a value of ~0.31. This is attributed to the occurrence of earlier recrystallization at 673K for the ECAP-processed materials as demonstrated in Fig. 4 [45].

5. Summary and conclusions

1. An Al-Zn-Mg alloy with a grain size of ~ 1.3 μm was processed by ECAP at 423 K from 1 to 8 passes and then tested dynamically at a strain rate of 4000 s^{-1} at temperatures from RT to 673 K.

2. Processing by ECAP produced fairly homogeneous grain structures with average grain sizes of ~200 and ~190 nm after ECAP through 4 and 8 passes, respectively. The as-received alloy contained GP zones and coarse plate-like η′. The experiments show the η′ phase is refined a η phase is formed during the first pass of ECAP and after further processing to 8 passes the GP zones are removed. In addition, dynamic straining at a high strain rate assists the precipitation process through dynamic precipitation, the coalescence of precipitates and through changes in the precipitate orientations.

3. The dynamic compressive yield strengths and flow stresses of the as-received and the ECAP-processed alloy decrease gradually to different degrees with increasing temperature, except for the alloy after 4 passes of ECAP which exhibit thermal stability up to 473 K due to the presence of nano-sized η′ and η precipitates which restrict grain boundary migration and recrystallization.

4. Excellent mechanical properties were achieved after processing the alloy by ECAP. Both the yield strength and peak stress were superior by comparison with the as-received material when dynamically deformed at temperatures ranging from RT to 673 K. Specifically, in the interval from 373 to 673 K the flow stresses after 4 passes of ECAP was ~150 MPa higher than in the as-received alloy.

Acknowledgements

References

[1] H.T. Lee, G.H. Shaue, The thermomechanical behavior for aluminum alloy under uniaxial tensile loading, Mater. Sci. Eng. A 268 (1999) 154-164.

[2] J.M. García-Infanta, A.P. Zhilyaev, A. Sharafutdinov, O.A. Ruano, F. Carreño, An evidence of high strain rate superplasticity at intermediate homologous temperatures in an Al–Zn–Mg–Cu alloy processed by high-pressure torsion, J. Alloys Compd. 473 (2009) 163-166.

[3] C.M. Cepeda-Jiménez, J.M. García-Infanta, M. Pozuelo, O.A. Ruano, F. Carreño, Impact toughness improvement of high-strength aluminium alloy by intrinsic and extrinsic fracture mechanisms via hot roll bonding, Scripta Mater. 61 (2009) 407-410.

[4] R. Jayaganthan, H.-G. Brokmeier, B. Schwebke, S.K. Panigrahi, Microstructure and texture evolution in cryorolled Al 7075 alloy, J. Alloys Compd. 496 (2010) 183-188.

[5] R.Z. Valiev, R.K. Islamgaliev, I.V. Alexandrov, Bulk nanostructured materials from severe plastic deformation, Prog. Mater. Sci. 45 (2000) 103-189.

[6] R.Z. Valiev, T.G. Langdon, Principles of equal-channel angular pressing as a processing tool for grain refinement, Prog. Mater. Sci. 51 (2006) 881-981.

[7] A.P. Zhilyaev, T.G. Langdon, Using high-pressure torsion for metal processing: Fundamentals and applications, Prog. Mater. Sci. 53 (2008) 893-979.

[8] Z. Horita, T. Fujinami, T.G. Langdon, The potential for scaling ECAP: effect of sample size on grain refinement and mechanical properties, Mater. Sci. Eng. A 318 (2001) 34-41.

[9] J. Wang, Y. Iwahashi, Z. Horita, M. Furukawa, M. Nemoto, R.Z. Valiev, T.G. Langdon, An investigation of microstructural stability in an Al-Mg alloy with submicrometer grain size, Acta Mater. 44 (1996) 2973-2982.

[10] Y. Iwahashi, Z. Horita, M. Nemoto, T.G. Langdon, An investigation of microstructural evolution during equal-channel angular pressing, Acta Mater. 45 (1997) 4733-4741.

[11] Y. Iwahashi, Z. Horita, M. Nemoto, T.G. Langdon, The process of grain refinement in equal-channel angular pressing, Acta Mater. 46 (1998) 3317-3331.

[12] Z. Horita, T. Fujinami, M. Nemoto, T.G. Langdon, Improvement of mechanical properties for Al alloys using equal-channel angular pressing, J. Mater. Process. Technol. 117 (2001) 288-292.

[13] J. Gubicza , I. Schiller , N.Q. Chinh , J. Illy , Z. Horita , T.G. Langdon, The effect of severe plastic deformation on precipitation in supersaturated Al-Zn-Mg alloys, Mater. Sci. Eng. A 460-461 (2007) 77-85.

[14] K. Ma, H. Wen , T. Hu, T.D. Topping , D. Isheim, D. N. Seidman , E. J. Lavernia , J.M. Schoenung, Mechanical behavior and strengthening mechanisms in ultrafine grain precipitation-strengthened aluminum alloy, Acta Mater. 62 (2014) 141-155.

[15] M.H. Shaeri, M.T. Salehi, S.H. Seyyedein, M.R. Abutalebi, J.K. Park, Microstructure and mechanical properties of Al-7075 alloy processed by equal channel angular pressing combined with aging treatment, Mater. Des. 57 (2014) 250-257.

[16] Y. Duan, L. Tang , G. Xu, Y. Deng, Z. Yin, Microstructure and mechanical properties of 7005 aluminum alloy processed by room temperature ECAP and subsequent annealing, J. Alloys Compd. 664 (2016) 518-529.

[17] Y. Xiong , N. Li, H. Jiang, Z. Li, Z. Xu, L. Liu, Microstructural evolutions of AA7055 aluminum alloy under dynamic and quasi-static compressions, Acta Metall. Sin. (Engl. Lett.) 27 (2014) 272-278.

[18] M. Furukawa, Y. Iwahashi, Z. Horita , M. Nemoto, T.G. Langdon, The shearing characteristics associated with equal-channel angular pressing, Mater. Sci. Eng. A 257 (1998) 328-332.

[19] Y. Iwahashi, J. Wang. Z. Horita, M. Nemoto, T.G. Langdon, Prionciple of equal-channel angular pressing for the processing of ultra-fine grained materials, Scr. Mater. 35;1996:143-146.

[20] L. Wang, Y.C. Wang, A.P. Zhilyaev, A.V. Korznikov, S. Li, E. Korznikova, T.G. Langdon, Dynamic compressive behavior of ultrafine-grained pure Ti at elevated temperatures after processing by ECAP, J. Mater. Sci. 49 (2014) 6640-6647.

[21] G. Sha, A. Cerezo, Early-stage precipitation in Al-Zn-Mg-Cu alloy (7050), Acta Mater. 52 (2004) 4503-4516.

[22] A. Kverneland, V. Hansen, R. Vincent, K. Gjønnes, J. Gjønnes, Structure analysis of embedded nano-sized particles by precession electron diffraction. η'-precipitate in an Al-Zn-Mg alloy as example, Ultramicroscopy 106 (2006) 492-502.

[23] M.H. Shaeri, M. Shaeri, M. Ebrahimi, M.T. Salehi, S.H. Seyyedein, Effect of ECAP temperature on microstructure and mechanical properties of Al-Zn-Mg-Cu alloy, Prog. Nat. Sci. 26 (2016) 182-191.

[24] L.K. Berg, J. Gjønnes, V. Hansen, X. Z.Li, M. K.-Wedel, G. Waterloo, D. Schryvers, L. R. Wallenberg, GP-zones in Al-Zn-Mg alloys and their role in artificial aging, Acta Mater. 49 (2001) 3443–3451.

[25] G. Sha, Y.B. Wang, X.Z. Liao, Z.C. Duan, S.P. Ringer, T.G. Langdon, Influence of equal-channel angular pressing on precipitation in an Al–Zn–Mg–Cu alloy, Acta Mater. 57 (2009) 3123-3132.

[26] Z.H. Li, B.Q. Xiong, Y.A. Zhang, B.H. Zhu, F. Wang, H.W. Liu, Microstructural evolution of aluminum alloy 7B04 thick plate by various thermal treatments, Trans. Nonferrous Met. Soc. China 18 (2008) 40-45.

[27] A.C. Chou, On the precipitation of η' phase in an Al-Zn-Mg alloy, Scripta Metall. 12 (1978) 421-423.

[28] J. Gjønnes, C. J. Simensen, An electron microscope investigation of the microstructure in an Aluminium-Zinc-Magnesium alloy, Acta Metall.18 (1970) 881-890.

[29] J. Gubicza, G. Ribárik, G.R. Goren-Muginstein, A.R. Rosen, T. Ungár, The density and the character of dislocations in cubic and hexagonal polycrystals determined by X-ray diffraction, Mater. Sci. Eng. A 309-310 (2001) 60-63.

[30] R. Howard, N. Bogh, D. S. MacKenzie, Heat Treating Processes and Equipment, in: G. E. Totten, D. S. MacKenzie (Eds.), Handbook of Aluminum Volume 1 Physical Metallurgy and Processes, Marcel Dekker, New York, 2003, 911-920.

[31] C. Xu, M. Furukawa, Z. Horita, T.G. Langdon, Using ECAP to achieve grain refinement, precipitate fragmentation and high strain rate superplasticity in a spray-cast aluminum alloy, Acta Mater. 51 (2003) 6139-6149.

[32] M. Murayama, Z. Horita, K. Hono, Microstructure of two-phase Al-1.7 at% Cu alloy deformed by equal-channel angular pressing, Acta Mater. 49 (2001) 21-29.

[33] I. Gutierrez-Urrutia, M.A. Muñoz-Morris, D.G. Morris, The effect of coarse second-phase particles and fine precipitates on microstructure refinement and mechanical properties of severely deformed Al alloy, Mater. Sci. Eng. A 394 (2005) 399-410

[34] C. Xu, M. Furukawa, Z. Horita, T.G. Langdon, Influence of ECAP on precipitate distributions in a spray-cast aluminum alloy, Acta Mater. 53 (2005) 749-758

[35] Y. Gao, Z. Zhuang, Z.L. Liu, X.C. You, X.C. Zhao, Z.H. Zhang, Investigations of pipe-diffusion-based dislocation climb by discrete dislocation dynamics, Int. J. Plasticity 27 (2011) 1055-1071.

[36] T. Hu, K. Ma, T.D. Topping, J.M. Schoenung, E.J. Lavernia, Precipitation phenomena in an ultrafine-grained Al alloy, Acta Mater. 61 (2013) 2163-2178.

[37] U.F. Kocks, H. Mecking, Physics and phenomenology of strain hardening: The FCC case, Prog. Mater Sci. 48 (2003) 171-273.

[38] J. G. Sevillano, P. vanHoutte, E. Aernoudt, Large strain work-hardening and textures, Prog. Mater Sci. 25 (1980) 69–412.

[39] A.S. Argon, P. Haasen, A new mechanism of work-hardening in the late stages of large-strain plastic flow in F.C.C. and diamond cubic crystals, Acta Metall. Mater. 41 (1993) 3289-3306.

[40] A. Deschamps, M. Niewczas, F. Bley,Y. Brechet, J. D. Embury, L. L. Sinq, F. Livet, J. P. Simon, Low-temperature dynamic precipitation in a supersaturated Al-Zn-Mg alloy and related strain hardening, Philos. Mag. A 79 (1999) 2485-2504.

[41] S. K. Moghanaki, M. Kazeminezhad, Modeling of the mutual effect of dynamic precipitation and dislocation density in age hardenable aluminum alloys, J. Alloys Compd. 683 (2016) 527–532.

17

 [42] L.M. Cheng, W.J. Poole, J.D. Embury, D.J. Lloyd, The Influence of Precipitation on the Work-Hardening Behavior of the Aluminum Alloys AA6111 and AA7030, Metall. Mater. Trans. A 34 (2003) 2473-2481.

[43] P. H.-Benhangi, M. Mazinani, M. H.-Sabzevar, Physically Based Model of the Yield Strength for an Al-Mg-Si-Cu-Zn Alloy, Metall. Mater. Trans. A. 46 (2015) 5407–5417.

[44] S. Zhang, Y.C. Wang, A.P. Zhilyaev, D. V. Gunderov, S. Li, G.I. Raab, E. Korznikova, T.G. Langdon, Effect of temperature on microstructural stabilization and mechanical properties in the dynamic testing of nanocrystalline pure Ti, Mater. Sci. Eng. A. 634 (2015) 64–70.

[45] G. Z. Quan, Y.P. Mao, G.-S. Li, W.Q. Lv, Y. Wang, J. Zhou, A characterization for the dynamic recrystallization kinetics of as-extruded 7075 aluminum alloy based on true stress - strain curves, Comput. Mater. Sci. 55 (2012) 65–72.

Table 1. Summary of microstructural features observed in the as-received and ECAP processed Al-Zn-Mg alloy.

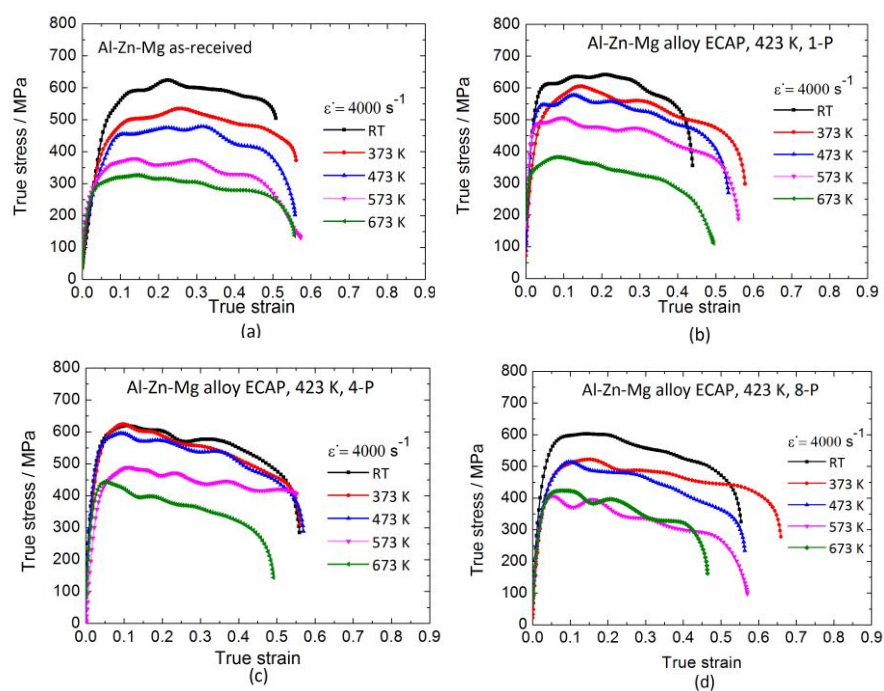|	As-received		1 ECAP pass		4 ECAP passes		8 ECAP passes	
Average grain size	1.3 μm		800 nm in width		200 nm		190 nm	
Precipitates Type	GP zones	η'	GP zones	η'	η'	η	η'	η
Precipitates Morphology	spherical	Plate-like	spherical	Plate-like	spherical	Oval-like	spherical	Oval-like
Precipitates size (nm)	5	120	3.9	5(120)	13	60	18	65
Dislocations density (m^{-2})	2.5×10^{13}		3.5×10^{14}		3.2×10^{14}		3.25×10^{14}	

Fig. 1 True stress-strain curves of Al-Zn-Mg alloy deformed at 4000 s^{-1}: (a) as-received and after

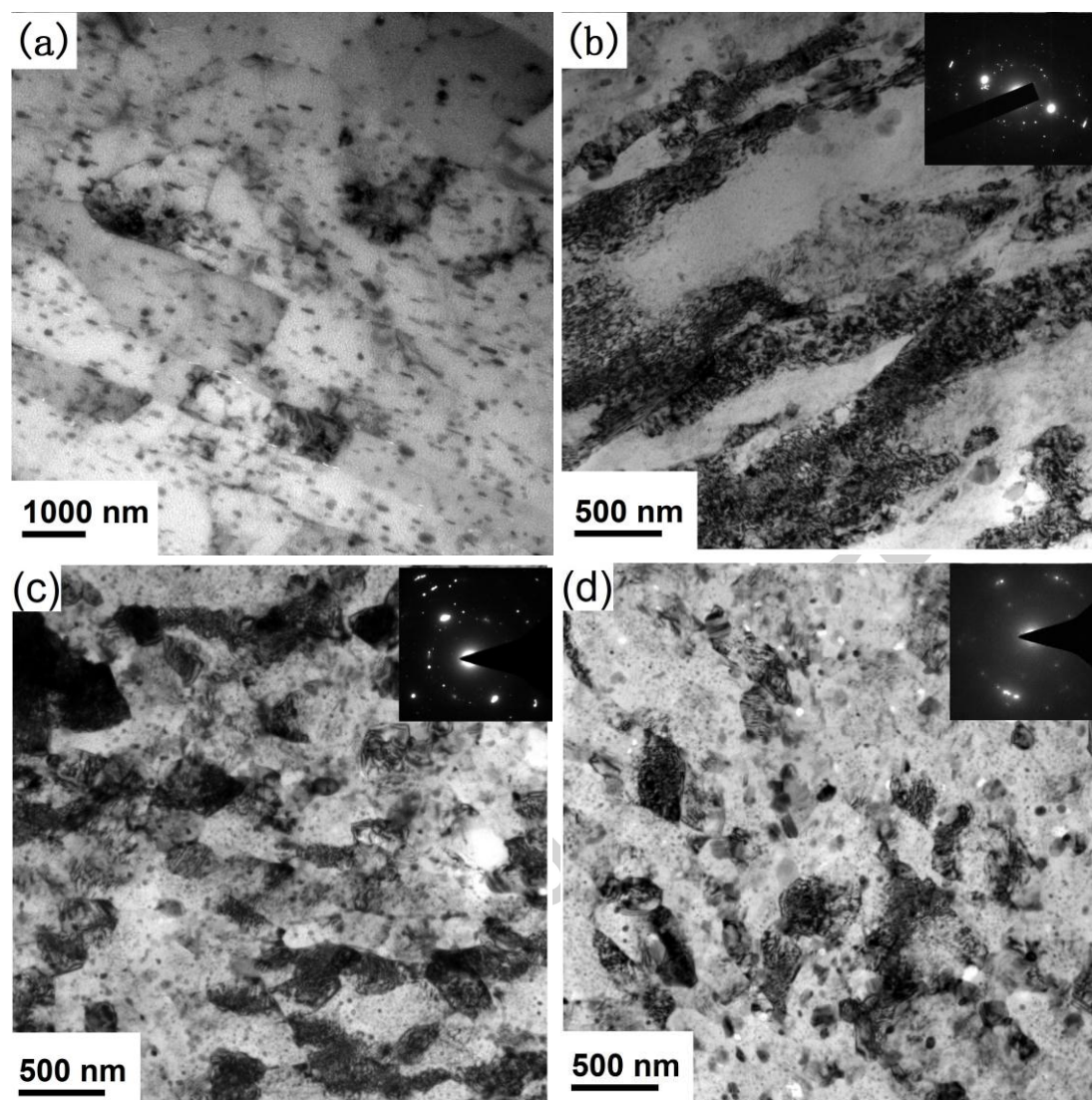ECAP for (b) 1 pass, (c) 4 passes and (d) 8 passes.

Fig. 2 TEM micrographs of the alloy (a) as-received and after ECAP for (b) 1 pass, (c) 4 passes and (d) 8 passes.
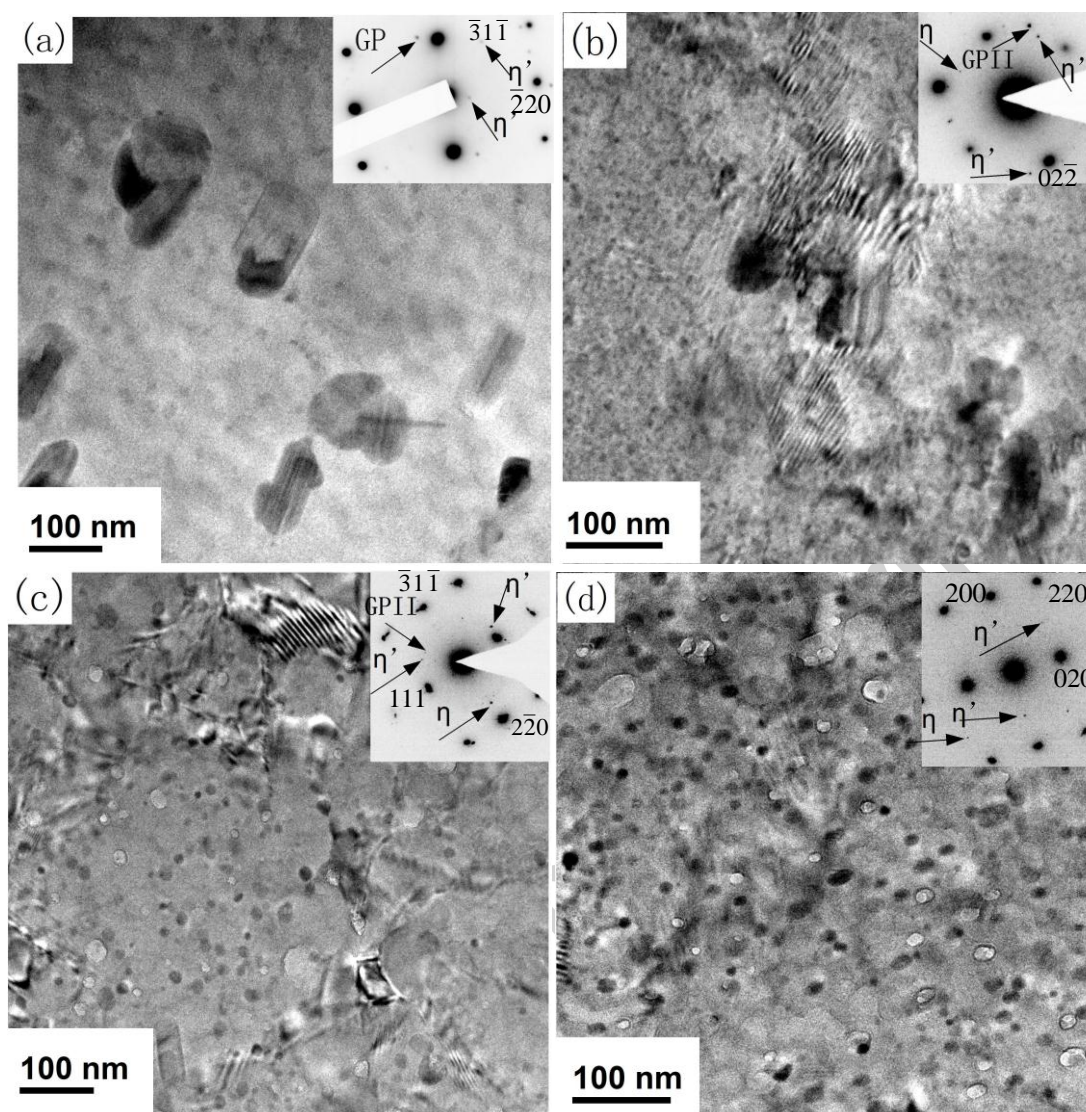
Fig. 3 TEM micrographs of Al-Zn-Mg alloy and corresponding SAED patterns (a) as-received and after ECAP for (b) 1 pass, (c) 4 passes and (d) 8 passes.
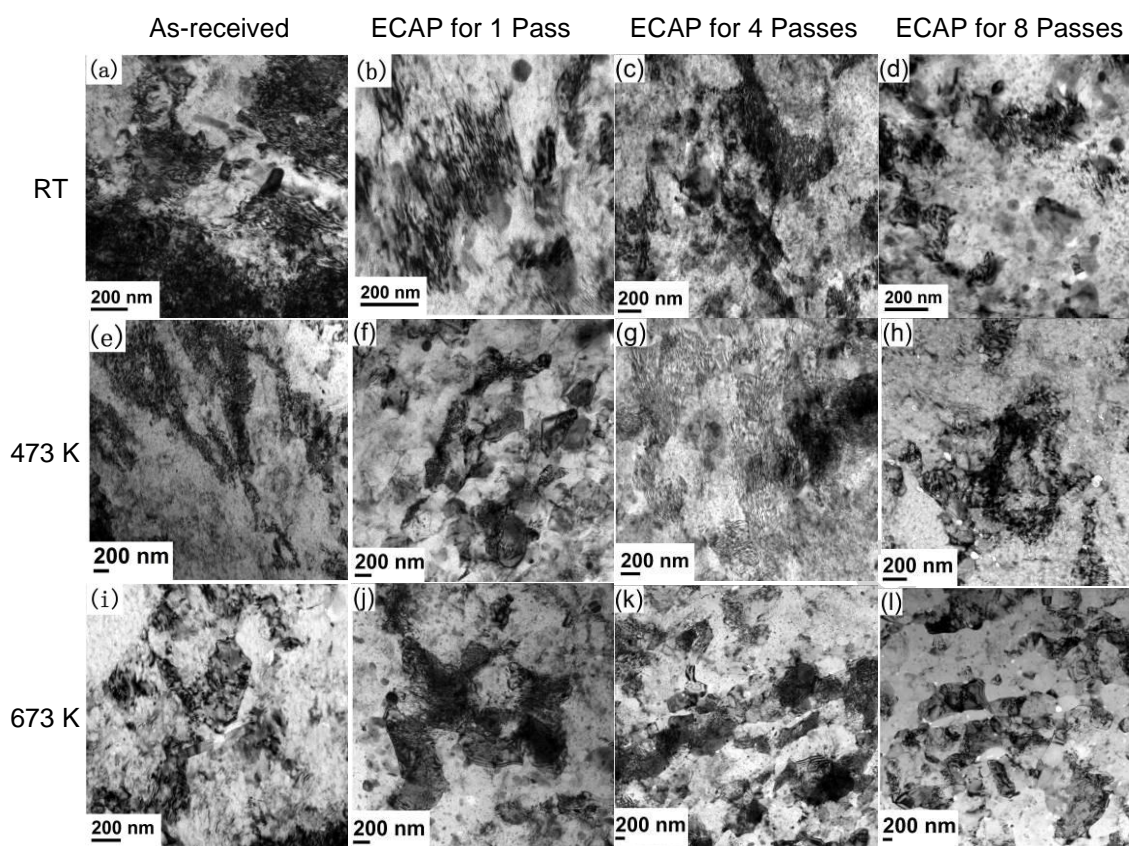
Fig. 4 Representative micrographs of the alloy processed by ECAP and then dynamically tested at 4000 s^{-1} at RT (top row), 473 (middle row) and 673 K (bottom row).

Fig. 5 SAED patterns of Al-Zn-Mg alloy processed by ECAP and then dynamically tested at 4000 s^{-1} and at RT (top row), 473 (middle row) and 673 K (bottom row).
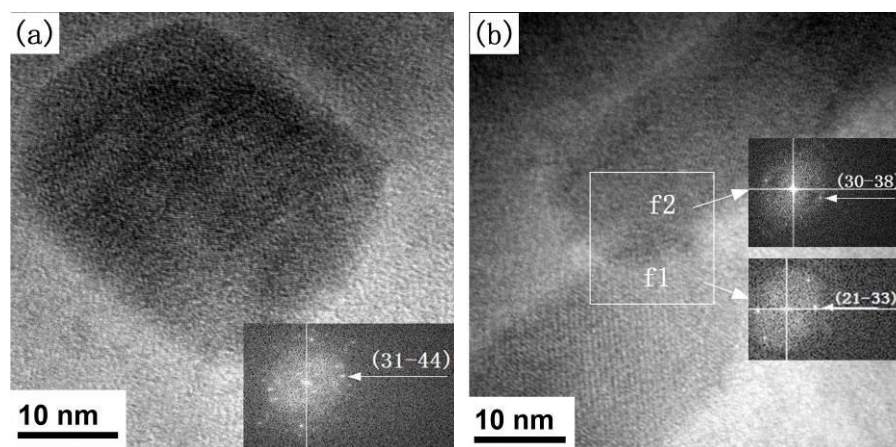
Fig. 6 TEM and FFT of (a) η' precipitates in the as-received Al-Zn-Mg alloy tested at 673 K and (b) two η'

precipitates in the alloy processed by 1 pass of ECAP and then tested at 673 K.
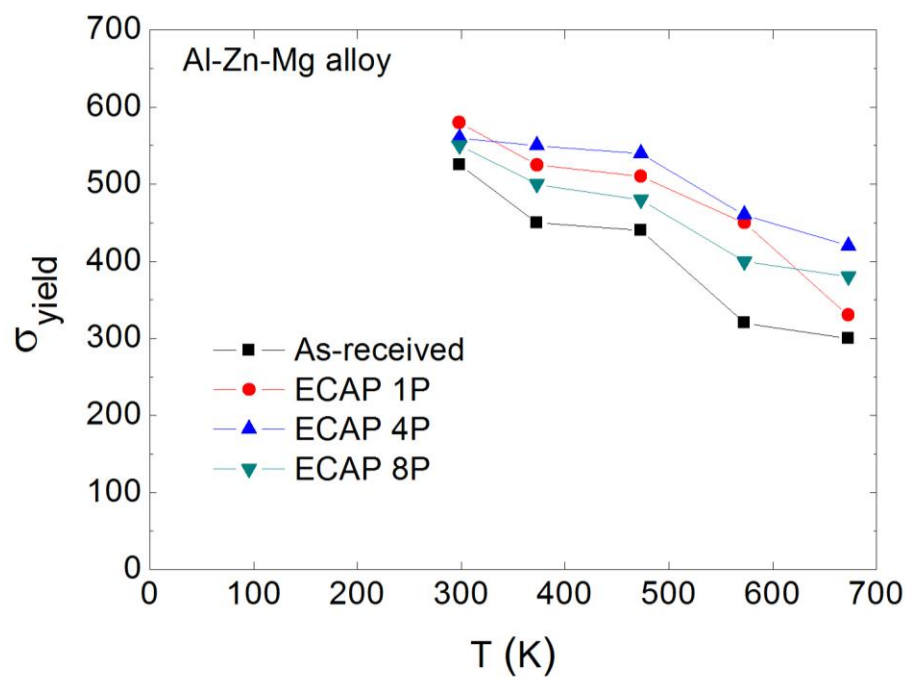
Fig. 7 Temperature dependence of the yield strength of the alloy in the as-received and ECAP-processed conditions.
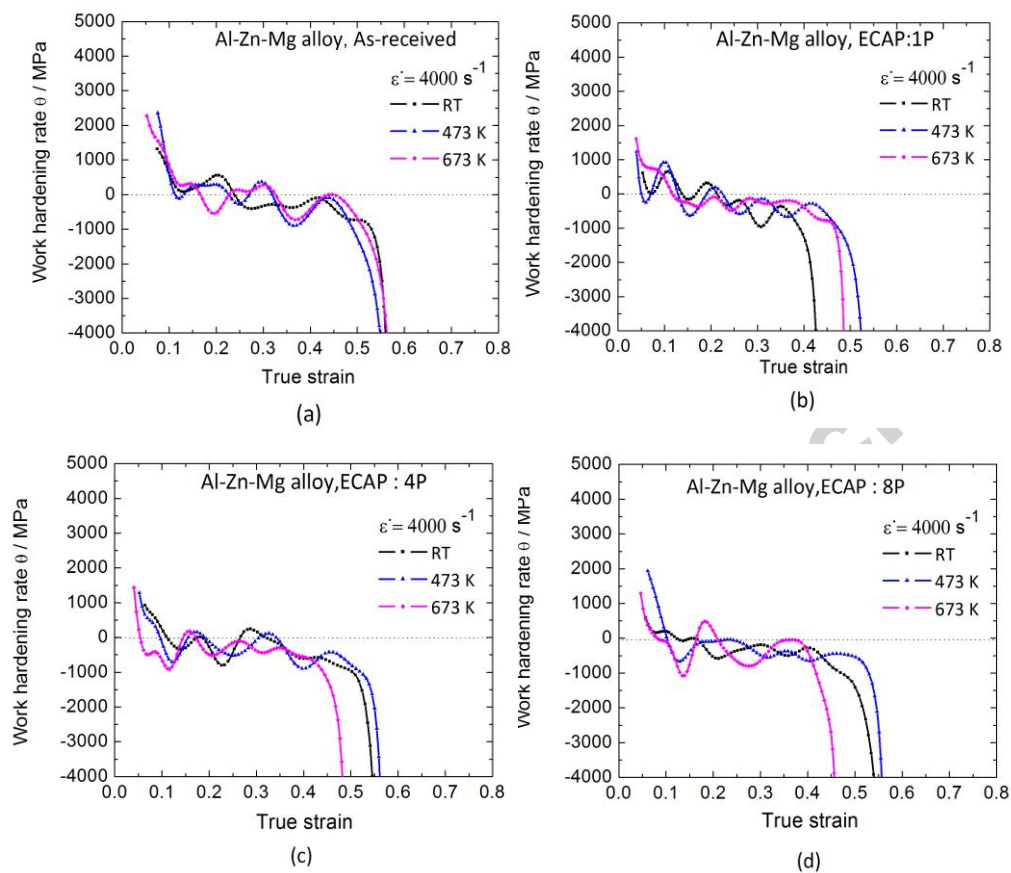
Fig. 8 Strain hardening rate vs. true strain for (a) as-received material and after ECAP through (b) 1, (c) 4 and (d) 8 passes of ECAP at different deformation temperatures with a strain rate of 4000 s^{-1}.